

FAST MAGNETIC SUSCEPTIBILITY RECONSTRUCTION USING L0 NORM OF GRADIENT

Weijun Liu¹, Jianzhong Lin², Congbo Cai¹, Delu Zeng¹ and Xinghao Ding^{*1}

¹Department of Communications Engineering, Xiamen University, Fujian, China

²Zhongshan Hospital Xiamen University, Fujian, China

E-mail: dxh@xmu.edu.cn

ABSTRACT

There is a growing interest in quantifying tissue susceptibility in MRI. However, the zeros in the dipole kernel makes the calculation of the magnetic susceptibility from the measured field to be an ill-posed problem. Recently, Bayesian regularization approaches have been utilized to enable accurate quantitative susceptibility mapping(QSM), such as L2 norm gradient minimization and TV. In this work, we propose an efficient QSM method by using a sparsity promoting regularization which called L0 norm of gradient to reconstruct susceptibility map. The use of L0 norm allows us to yield high quality image and prevent penalizing salient edges. Since the L0 minimization is an NP-hard problem, a special alternating optimization strategy by introducing an auxiliary variable is adopted to solve the problem and it only takes 1-2 mins to reconstruct the whole 3D susceptibility data. Both numerical phantom simulations and human brain tests are performed to demonstrate the superior performance of the proposed method compared with previous methods.

Index Terms— quantitative susceptibility mapping, ill-posed problem, L0 norm of gradient, alternating optimization

1. INTRODUCTION

Magnetic susceptibility is a physical property of material that can be used as contrast mechanism in magnetic resonance imaging(MRI)[1]. In the past decade, the magnetic susceptibility plays an increasingly significant role in the medical field. Different tissues have different magnetic susceptibility, such as calcium [2] and iron-laden tissue [3] and so on. Nowadays, susceptibility has been used to diagnosis sickle cell disease, aplastic anemia, thalassemia, hemochromatosis and Parkinson's disease.

Many relative techniques have focused on the magnetic susceptibility. The relationship between the magnetic susceptibility and observed phase in k-space was revealed in

[4]. However, the estimation of magnetic susceptibility from phase is an ill-posed problem due to the presence of zero value on a conical surface. In order to overcome this problem, a method called Thresholded K-space Division(TKD) [5] was introduced. This method is straightforward implementation, but it leads to inaccurate estimation in k-space regions where the threshold is applied. A more accurate technique to estimate the susceptibility is the COSMOS method [6]. The method is simple, but requires repeating the data acquisition at multiple orientations. Practically, it is difficult to rotate the body to acquire data. Recently there are many reconstruction methods using single orientation. These methods require prior knowledge to reconstruct susceptibility map. Since the susceptibility distribution is approximated to be piece-wise constant, the susceptibility map can be reconstructed by L2 gradient minimization or TV [7]. In addition, edge weights derived from the magnitude image or phase image are often employed to protect certain gradient [8, 9, 10, 11]. In [8], the authors introduced a magnitude-weighted L2 norm penalty on the spatial gradient of susceptibility map. In [9, 10], magnitude-weighted TV was used to yield better suppression of streaking artifacts than the method in [8]. In [11], Schweser et al. used edge information from phase and magnitude rather than only magnitude. The strategy using edge weighting may introduce erroneous contrast information due to the incomplete consistencies among the magnitude gradient, phase gradient and the gradient of the true susceptibility map.

In this paper, we use L0 term instead of L1 term to directly measure the gradient sparsity in the context of QSM. Compared with L1 norm, L0 norm is the ideal sparse representation and L1 norm is only the convex relaxation of L0 norm [12, 13]. The reconstruction time is also an important issue in MRI applications. In our model, since the L0 minimization is an NP-hard problem, it is hard to solve. Recently, Xu et al. provided an algorithm for directly solving the gradient minimization problem in the context of image smoothing [14]. Different to the 2D problem in [14], in our case, the susceptibility reconstruction problem takes place in 3D because of the three dimensional relationship between susceptibility and magnetic field. Here we solve the model by using alternating minimization algorithm. The computation time is only

The project is supported by the National Natural Science Foundation of China (No. 30900328, 61172179, 61103121, 81301278, 81171331), the Natural Science Foundation of Fujian Province of China (No. 2012J05160), the National Key Technology R&D Program (2012BAI07B06), the Fundamental Research Funds for the Central Universities (No. 2011121051, 2013121023, 2010121101).

1-2 minutes and comparable to the method in [15] where a ‘split Bregman’ method was used to fast QSM via TV. Numerical phantom simulations are performed to demonstrate the superior performance of the proposed method and human brain results illustrate that the method is suitable in practice.

2. THEORY

2.1. Susceptibility and Field

In Fourier space, the relationship between the susceptibility and the magnetic field can be represented as

$$B_k(k) = X_k(k) \bullet \left(\frac{1}{3} - \frac{k_z^2}{k^2} \right) \quad (1)$$

where B_k and X_k respectively represents the observed magnetic field and susceptibility distribution expressed in the Fourier domain, \bullet denotes point-wise multiplication, and $k^2 = k_x^2 + k_y^2 + k_z^2$, k_x , k_y and k_z are coordinates in k-space. Given the magnetic field, the susceptibility can be calculated with a direct inversion as following :

$$X_k(k) = B_k(k) \bullet D^{-1}(k) \quad (2)$$

where $D(k) = \frac{1}{3} - \frac{k_z^2}{k^2}$. The inversion from magnetic field to susceptibility is an ill-posed problem due to the conical surface region defined by $k_x^2 + k_y^2 = 2k_z^2$ (magic angle is 54.7°). In Fig.1, we show the axial, coronal and sagittal view of the dipole kernel in k-space. It is noticed that the susceptibility value tend to infinity on the surface in k-space. The noise and error detection arising from the local field in the region adjacent to the conical surface can be enhanced in the estimated susceptibility map.

2.2. The L0 minimization

We propose to solve the inverse problem by imposing prior knowledge on the reconstructed susceptibility map. Here L0 gradient is considered as a prior information. The L0 norm of gradient indicates the numbers of nonzero gradient. For a pixel of the three dimension MR signal X_p , it is considered as the following expression:

$$\|GX_p\|_0 = \# \{p \mid |G_x X_p| + |G_y X_p| + |G_z X_p| \neq 0\} \quad (3)$$

where G is the image gradient operator and $\#\{\}$ is the counting operator. The L0 norm of gradient returns 1 when $|G_x X_p| + |G_y X_p| + |G_z X_p| \neq 0$. For a non-zero a , $\|aGX_p\|_0 = \# \{p \mid |aG_x X_p| + |aG_y X_p| + |aG_z X_p| \neq 0\}$, it is equal to $\|GX_p\|_0$. This counting strategy is different from traditional smoothing method, such as TV, the non-zero a can affect the gradient magnitude. Due to this counting strategy, salient edges are automatically protected via L0 minimization while total variation imposes large penalties on salient gradients.

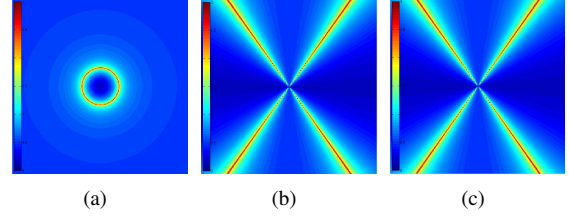


Fig. 1. The images of $\log(|D^{-1}|)$ in the axial(a), coronal(b) and sagittal(c) planes.

In the case of susceptibility reconstruction, we consider the following optimization problem:

$$\arg \min_X \left\| F^H DFX - B \right\|_2^2 + \lambda \|GX\|_0 \quad (4)$$

where F is 3-D Fourier transform, D is a diagonal matrix with entries $\frac{1}{3} - \frac{k_z^2}{k^2}$, B and X are the vectorized observed magnetic field and susceptibility distribution. Here we introduce auxiliary variable to relax the formula (4) and use alternating minimization algorithm to solve it. It can be posed as the unconstrained optimization problem:

$$\arg \min_X \left\| F^H DFX - B \right\|_2^2 + \lambda \|A\|_0 + \beta \|GX - A\|_2^2 \quad (5)$$

where $A = [A_x; A_y; A_z]$ is auxiliary variable corresponding to GX and β is an parameter to control the similarity between auxiliary variable and the corresponding component. First, fixing A , the susceptibility can be estimated through minimizing

$$\left\| F^H DFX - B \right\|_2^2 + \beta \|GX - A\|_2^2 \quad (6)$$

The susceptibility X in k-space domain can be directly found through diagonal matrix inversion and FFTs as

$$FX = [D^2 + \beta E^2]^{-1} [D^H FB + \beta E^H FA] \quad (7)$$

where $E = [E_x; E_y; E_z]$ represents difference operator in k-space domain [15] and E_x is a diagonal matrix with entries $E_x(i, i) = 1 - \exp(-2\pi\sqrt{-1}k_x(i, i)/N_x)$, where N_x is the matrix size along x axis. The operators E_y and E_z are similarly defined.

After solving FX , the second subproblem is to solve A by using the following representation:

$$\arg \min_A \lambda \|A\|_0 + \beta \|GX - A\|_2^2 \quad (8)$$

(8) has a closed-form solution to yield A by

$$A_i = \begin{cases} 0 & (G_x X)^2 + (G_y X)^2 + (G_z X)^2 \leq \frac{\lambda}{\beta} \\ G_i X & \text{otherwise} \end{cases} \quad (9)$$

where $i = x, y, z$ and all operations are done component-wisely. We repeat the two steps to achieve good result. The algorithm can be formulated as **Algorithm 1**. The parameter β starting from β_0 is multiplied by rate κ in each iteration so that convergence rate can be improved. The termination criterion is the change of susceptibility values in the adjacent iterations falls below 1%.

Algorithm 1

Input: normalized field shift B , convolution kernel D , rate κ , parameters λ, β_0 .

Initialization: $A \leftarrow 0, \beta \leftarrow \beta_0, i \leftarrow 0$.

repeat

With $A^{(i)}$, solve for $FX^{(i)}$ in Eq.(7).

With $FX^{(i)}$, solve for $A^{(i+1)}$ in Eq.(9).

$\beta \leftarrow \kappa\beta, i++$.

until $100 \times \frac{\|FX^{(i)} - FX^{(i-1)}\|_2^2}{\|FX^{(i)}\|_2^2} \leq 1\%$.

Output: susceptibility map X .

2.3. The L0 minimization with a physical prior

In order to protect edges in susceptibility image that correspond to edges in the magnitude image and overcome the lack of measurable field data at the magic angle, a physical prior was utilized to QSM [8, 9, 10, 11]. In our case, the minimization problem turns to be the following representation:

$$\arg \min_X \left\| F^H DFX - B \right\|_2^2 + \lambda \|MGX\|_0 \quad (10)$$

where M is a binary matrix which is derived from the gradient of the magnitude image. According to Liu et al. [10], the largest 30% gradients of the magnitude image in ROI are considered as edge in magnitude image.

3. MATERIALS AND RESULTS

To demonstrate the superiority of the proposed method, numerical phantom with known susceptibility and human brain data were utilized to perform the proposed method. Data processing was carried out using a 64-bit windows system with 2.4 GHz Dual Core Intel Xeon processor and 32 GB of RAM in Matlab (The Mathworks Inc, Massachusetts).

3.1. Numerical phantom simulation

A 3D numerical phantom experiment was carried out to evaluate the accuracy of our proposed method. The numerical phantom consisted of a $240 \times 240 \times 154$ image with resolution $1 \times 1 \times 1 \text{ mm}^3$, and the susceptibilities were set to different values in three compartments (gray and white matter, csf). The susceptibility values in these compartments were defined as: $X_{white} = -0.2 \text{ ppm}$, $X_{gray} = 0.2 \text{ ppm}$ and $X_{csf} = -0.1 \text{ ppm}$. The susceptibility of background was set to zero (Fig.2(a)). The field map was calculated (Fig.2(b)) and zero mean Gaussian noise was added to obtain the noisy field map (Fig.2(c)). Finally the susceptibility image was reconstructed and we used normalized root-mean-square error (RMSE) as a metric to quantify the error in the ROI obtained from different methods. The λ corresponding to the minimization of the reconstruction error was considered optimal.

In Fig.2, the calculated susceptibility maps using TKD (d), L2-reg (e), TV (f) and L0-reg (g) are shown in axial

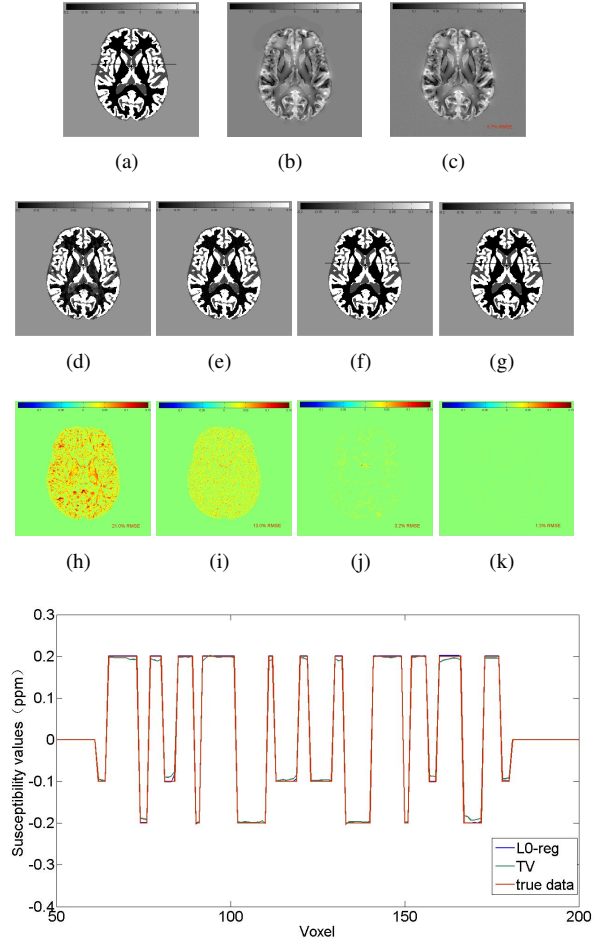


Fig. 2. Simulation validation of susceptibility maps with TKD (d), L2-reg (e), TV (f) and the proposed method (g). Ground truth susceptibility, field map and noisy field map are shown in (a-c). The third row shows the corresponding absolute error maps (h-k). The bottom row shows the 1D results from the 110-th row of the true data(a), TV result(f) and L0-reg result(g) respectively.

plane. The RMSE over the three compartments was 21.0%, 13.0%, 3.2% and 1.3% for TKD, L2-reg, TV and L0-reg, respectively. It can be seen that TKD method and L2-reg introduce obvious streaking artifacts and noise. The L0-reg result shows a high degree of similarity with TV by visual inspection. By close examination of the difference of two approaches, we compare the absolute error maps (Fig.2(j) and Fig.2(k)) and present susceptibility values in the 110-th row. It is obvious that the underestimation of structure edges is existed in TV method while it does not happen in L0 method. The mean value and stand variation in three compartments using these methods are shown in Table.1. The L0 minimization also provides more accurate susceptibility values than the other methods. In Fig.3, we show the Fourier spectra of the susceptibility maps and the corresponding error

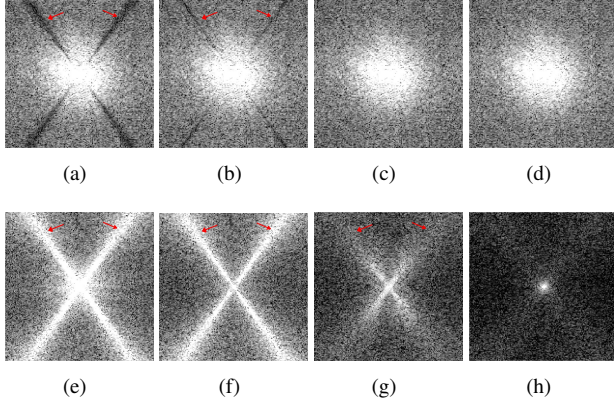


Fig. 3. Comparison of the proposed method with previous methods in the Fourier domain. In the sagittal view, the Fourier spectra corresponding to TKD (a), L2-reg (b), TV (c) and the proposed method (d) are illustrated in the top row. The bottom row shows the reconstruction error in the Fourier domain (e-h) respectively.

Table 1. Susceptibility measurement of three compartments using different methods.

	WM(ppm)	GM(ppm)	CSF(ppm)
Reference	-0.200	0.200	-0.100
TKD	-0.185±0.036	0.182±0.035	-0.091±0.036
L2-reg	-0.196±0.023	0.195±0.023	-0.094±0.023
L1-reg	-0.198±0.005	0.198±0.005	-0.096±0.007
L0-reg	-0.199±0.001	0.200±0.002	-0.099±0.004

maps, respectively. It can be seen that the error has a slightly higher energy level around the conical surface than in the surrounding regions in k-space. The Fourier spectra of TKD and L2-reg results revealed decreased Fourier coefficients in the ill-conditioned regions (red arrows). Although TV performs better than the above two methods, it also can not recover the energy completely. This problem can be solved by the proposed method, as can be seen in Fig.3(h).

3.2. Human brain experiments

Here we used original data from Cornell MRI Research Lab in the relative website (<http://weill.cornell.edu/mri/pages/qsm.html>). The data were acquired on a 3.0T Siemens scanners with 8 echoes. The resolution was $0.9375 \times 0.9375 \times 2 \text{ mm}^3$ with a matrix of $256 \times 256 \times 62$. The shortest echo time was 3.6 ms with a 5.9 ms increment for the other 7 echoes. A region growing algorithm [16] was performed to unwrap the wrapped phase. The background field was removed by solving the Laplace equation with specified boundary values(LBV)[17]. After the background magnetic field removal, the susceptibility was calculated by solve formula (5) and formula (10). Based on the L-curve heuristic [18], the

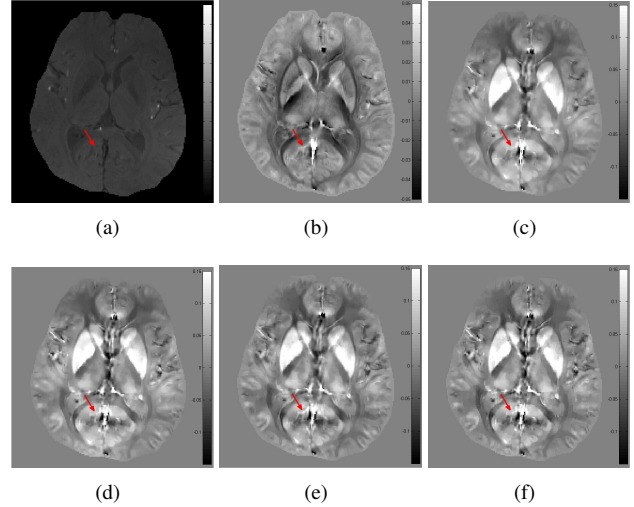


Fig. 4. Human brain QSM. Magnitude and local field are shown in (a), (b), respectively. The results from TV method (c), magnitude-weighted TV (d), L0-reg (e) and magnitude-weighted L0-reg (f) are shown for comparisons. Red arrows mark Vessel ROI.

regularization parameter λ corresponding to the corner of the L-curve was considered as the optimal one.

Comparisons of different susceptibility reconstruction methods from human brain in axial view are shown in Fig.4. The filtered field map from LBV(Fig.4(b)) was free of artifacts and provided additional anatomical details complementary to the magnitude image(Fig.4(a)). Both TV(Fig.4(c)) and L0 minimization (Fig.4(e)) can successfully generated QSMs. The iron-rich structures with high paramagnetic values are clearly visible in susceptibility maps. The main difference is the contrast of vessel which is indicated by red arrow. One of the causes may be the edge-preserve nature of L0 minimization in QSM. Since the magnitude and susceptibility maps do not always share completely same structure, it is very cautious to determine the number of zeros on the diagonal of M . Inaccurate weighting matrix may blur the structure and provide incorrect contrast, as shown in Fig.4(d) and Fig.4(f).

4. CONCLUSIONS

In this study, we propose a novel method for susceptibility reconstruction. The proposed L0 minimization method takes advantage of the ideal sparse representation of spatial variation in susceptibility maps. Numerical phantom experiments and in-vivo experiments confirm that the proposed method can accurately measure susceptibility and has better performance than TV in terms of edge-preserving. The computation of 3D susceptibility maps can be performed in a few minutes. For further research, more accurate edge-weighting will be explored to improve the quality of susceptibility image. We hope this method can be used for clinical applications.

5. REFERENCES

- [1] Bryan Kressler, Ludovic de Rochefort, Tian Liu, Pascal Spincemaille, Quan Jiang, and Yi Wang, "Nonlinear regularization for per voxel estimation of magnetic susceptibility distributions from mri field maps," *Medical Imaging, IEEE Transactions on*, vol. 29, no. 2, pp. 273–281, 2010.
- [2] Naoaki Yamada, Satoshi Imakita, Toshiharu Sakuma, and Makoto Takamiya, "Intracranial calcification on gradient-echo phase image: depiction of diamagnetic susceptibility.," *Radiology*, vol. 198, no. 1, pp. 171–178, 1996.
- [3] Robert J Ogg, James W Langston, E Mark Haacke, R Grant Steen, and June S Taylor, "The correlation between phase shifts in gradient-echo mr images and regional brain iron concentration," *Magnetic resonance imaging*, vol. 17, no. 8, pp. 1141–1148, 1999.
- [4] Rares Salomir, Baudouin Denis de Senneville, and Chrit TW Moonen, "A fast calculation method for magnetic field inhomogeneity due to an arbitrary distribution of bulk susceptibility," *Concepts in Magnetic Resonance Part B: Magnetic Resonance Engineering*, vol. 19, no. 1, pp. 26–34, 2003.
- [5] Sam Wharton, Andreas Schäfer, and Richard Bowtell, "Susceptibility mapping in the human brain using threshold-based k-space division," *Magnetic Resonance in Medicine*, vol. 63, no. 5, pp. 1292–1304, 2010.
- [6] Tian Liu, Pascal Spincemaille, Ludovic de Rochefort, Bryan Kressler, and Yi Wang, "Calculation of susceptibility through multiple orientation sampling (cosmos): a method for conditioning the inverse problem from measured magnetic field map to susceptibility source image in mri," *Magnetic Resonance in Medicine*, vol. 61, no. 1, pp. 196–204, 2009.
- [7] Leonid I Rudin, Stanley Osher, and Emad Fatemi, "Nonlinear total variation based noise removal algorithms," *Physica D: Nonlinear Phenomena*, vol. 60, no. 1, pp. 259–268, 1992.
- [8] Ludovic de Rochefort, Tian Liu, Bryan Kressler, Jing Liu, Pascal Spincemaille, Vincent Lebon, Jianlin Wu, and Yi Wang, "Quantitative susceptibility map reconstruction from mr phase data using bayesian regularization: validation and application to brain imaging," *Magnetic Resonance in Medicine*, vol. 63, no. 1, pp. 194–206, 2010.
- [9] Jing Liu, Tian Liu, Ludovic de Rochefort, James Ledoux, Ildar Khalidov, Weiwei Chen, A John Tsiouris, Cynthia Wisnieff, Pascal Spincemaille, Martin R Prince, et al., "Morphology enabled dipole inversion for quantitative susceptibility mapping using structural consistency between the magnitude image and the susceptibility map," *Neuroimage*, vol. 59, no. 3, pp. 2560–2568, 2012.
- [10] Tian Liu, Weiyu Xu, Pascal Spincemaille, Amir Salman Avestimehr, and Yi Wang, "Accuracy of the morphology enabled dipole inversion (medi) algorithm for quantitative susceptibility mapping in mri," *Medical Imaging, IEEE Transactions on*, vol. 31, no. 3, pp. 816–824, 2012.
- [11] Ferdinand Schweser, Karsten Sommer, Andreas Deistung, and Jürgen Rainer Reichenbach, "Quantitative susceptibility mapping for investigating subtle susceptibility variations in the human brain," *Neuroimage*, vol. 62, no. 3, pp. 2083–2100, 2012.
- [12] David L Donoho, "For most large underdetermined systems of linear equations the minimal ℓ_1 -norm solution is also the sparsest solution," *Communications on pure and applied mathematics*, vol. 59, no. 6, pp. 797–829, 2006.
- [13] David L Donoho, "Compressed sensing," *Information Theory, IEEE Transactions on*, vol. 52, no. 4, pp. 1289–1306, 2006.
- [14] Li Xu, Cewu Lu, Yi Xu, and Jiaya Jia, "Image smoothing via ℓ_0 gradient minimization," *ACM Transactions on Graphics (TOG)*, vol. 30, no. 6, pp. 174, 2011.
- [15] Berkin Bilgic, Audrey P Fan, Jonathan R Polimeni, Stephen F Cauley, Marta Bianciardi, Elfar Adalsteinsson, Lawrence L Wald, and Kawin Setsompop, "Fast quantitative susceptibility mapping with ℓ_1 -regularization and automatic parameter selection," *Magnetic Resonance in Medicine*, 2013.
- [16] R Cusack and N Papadakis, "New robust 3-d phase unwrapping algorithms: application to magnetic field mapping and undistorting echoplanar images," *Neuroimage*, vol. 16, no. 3, pp. 754–764, 2002.
- [17] Dong Zhou, Tian Liu, Pascal Spincemaille, and Yi Wang, "Background field removal by solving the laplacian boundary value problem," *NMR in Biomedicine*, vol. 27, no. 3, pp. 312–319, 2014.
- [18] Per Christian Hansen, *The L-curve and its use in the numerical treatment of inverse problems*, IMM, Department of Mathematical Modelling, Technical University of Denmark, 1999.